sciendo
Polish Journal of Medical Physics and Engineering
The Journal of Polish Society of Medical Physics
ISSN 1898-0309, doi: 10.2478/pjmpe-2025-0026
September 2025
Vol 31, Issue 3

Scientific Paper

Evaluating scintigraphic dyssynchrony as radiomic parameters for dynamic laminar and turbulent fluids in compartmental phantom systems: A signal processing study

Ahmad Alenezi [1, ABCDEF*]

[1]*Radiologic Sciences Department, Kuwait University, Kuwait City 31470, Kuwait*
**Corresponding author: Ahmad Alenezi; ahmad.alenezi1@ku.edu.kw*

(received 14 February 2025; revised 12 April, 1 June 2025; accepted 24 July 2025)

Abstract

Introduction: Radiomics quantify radiological data to correlate with clinical findings. Dyssynchrony, a proposed radiomic parameter measured via phase images, reflects the temporal discoordination of ventricular contraction, which can impair overall cardiac efficiency. This study assessed the consistency and reliability of dyssynchrony in laminar and turbulent flow compartments under varying image acquisition. It also evaluated the relationship between dyssynchrony and fluid dynamics alterations.

Methods: The dataset included 64 dynamic images using gamma camera (128,000 frames) generated using an in-home phantom, representing combinations of flow velocity, count, and frame rates. Phase and amplitude images were generated and analyzed to calculate synchrony, entropy, approximate entropy (ApEn), and bounded-ApEn for different rotation directions. Entropy values were examined under parameter changes, with comparisons using Pearson's test, ANOVA, logistic regression, and receiver operating characteristic (ROC) analysis.

Results: Images were categorized by activity concentrations: Group 1 (37 MBq), Group 2 (29.5 MBq), and Group 3 (18.5 MBq). Group 1 showed a strong negative correlation between entropy and frame rates ($r = -0.991$, $p < 0.001$), while Group 3 displayed positive correlations between frame rate, ApEn, gray count, and pixel count. Logistic regression predicted turbulence (AUC = 0.93) and direction (AUC = 0.96) using bounded-ApEn. Regression analysis indicated ApEn and bounded-ApEn significantly predicted vortex parameters ($R^2 = 93\%$).

Conclusion: Dyssynchrony metrics, including entropy, ApEn, and bounded-ApEn, demonstrated consistent measurements across varying conditions. These findings highlight their potential for enhancing diagnostic accuracy and guiding personalized therapeutic strategies for conditions influenced by blood flow patterns

Keywords: radiomics, entropy, dyssynchrony, cardiac, phantom

Introduction

Radiomics represent quantitative values in radiological data correlated with clinical findings, and radiomics analysis comprises several steps including image acquisition, preprocessing, segmentation, and marker computation. Radiomics can capture tissue properties, including shape and heterogeneity, and may help evaluate cardiac abnormalities associated with dyssynchrony of tissue[1-3]. Originally used in oncology to assess tissue characteristics[4], which are linked to survival outcomes and cancer control challenges, radiomics can help capture cellular heterogeneity indices[4]. Unlike biopsies, which is invasive and provide limited information from a small tissue sample, radiomics studies offer a comprehensive view of tissue heterogeneity throughout the cardiac tissue[2]. It can help capture the severity of cardiac abnormalities and predict survival and treatment response[5]. Furthermore, the minimal nature of radiomic data supports the discovery of markers and patterns of disease evolution, progression, and treatment response. This imaging approach, which can utilize unstructured data from various modalities such as single photon emission tomography (SPECT), positron emission and computed tomography, and magnetic resonance imaging (MRI), enables the integration of radiomic data with clinical, laboratory, histological, and genomic information using unsupervised or supervised machine learning.

However, radiomics analysis performance remains unclear, including the evaluation of dyssynchrony. Entropy, a parameter of dyssynchrony, is a measure of uncertainty , particularly in

© 2025 Authors
This is an open access article licensed under the Creative Commons Attribution-NonCommercial-NoDerivs License (http://creativecommons.org/licenses/by-nc-nd/4.0/).

Authors' contribution:
A – Research concept and design, B – Collection and/or assembly of data, C – Data analysis and interpretation, D – Writing the article, E – Critical revision of the article, F – Final approval of the article.

specific areas of the heart, indicating changes in its functioning (contractility). For instance, entropy quantifies the temporal discoordination of ventricular contraction, which can impair overall cardiac efficiency of a target region of interest (ROI). The degree of chaos in this area is directly related to the extent of entropy, resulting in decreased predictability of the contraction and relaxation of the heart. This temporal discoordination may be a key characteristic of cardiac abnormalities[6-9]. Several cardiac imaging studies have advanced the understanding of ventricular dyssynchrony without considering the steps of radiomics analysis. O'Connell et al.[10] showed the efficacy of synchrony and entropy in radionuclide angiography for measuring ventricular synchrony, although with limited clinical implications. They did not discuss details concerning image acquisition that might affect the radiomics analysis. Jiménez-Ángeles et al.[11] observed that variations in radionuclide angiography phase imaging significantly influence synchrony and entropy readings, particularly in healthy individuals. However, they highlighted a lack of standardized measures regarding imaging parameters, underscoring a potential limitation in the methodology employed[11]. For instance, Nichols et al.[12] and Lalonde et al.[13] demonstrated the effectiveness of entropy and synchrony in radionuclide angiography (SPECT) for detecting dyssynchrony, despite concerns regarding manual segmentation and fixed ROIs. Contrastingly, Lalonde et al.[13] detected mechanical dyssynchrony in SPECT, although this study was limited by sample size and gating accuracy. Additionally, Johnson et al.[14] used SPECT, echocardiography, and MRI to identify patients with arrhythmogenic right ventricular cardiomyopathy but faced limitations owing to the small sample size and manual left ventricle (LV) segmentation. Similarly, the study lacked a clear standardization protocol for image processing. Additionally, most studies did not describe specific segmentation algorithms and did not evaluate the effects of changing acquisition parameters (or physiologic changes) on dyssynchrony parameters.

None of the previously mentioned studies followed the radiomics pipeline, including data acquisition, preprocessing, and image segmentation, that lead to accurate computation and image marker selection. Additionally, they lacked standardized protocols that may counteract reproducibility. This lack of reproducibility and validation of quantitative cardiac image analysis studies is a major challenge for nuclear cardiology. Additionally, among these studies, there was limited or no agreement in the reported dyssynchrony values. Establishing dyssynchrony as a radiomics must be performed carefully, as image acquisition data preprocessing/processing can significantly influence dyssynchrony results[15]. This standardization is crucial due to the arising interest in the entropy-related parameters as predictors for cardiac studies[16-18].

To address the challenges in dyssynchrony radiomics, this study aimed to examine certain radiomics parameters such as entropy, approximate entropy (ApEn), bounded-ApEn, and synchrony under various scenarios (i.e. different flow rate, count rate, frame rate, device rotation direction), to examine the impact of the direction of rotation and various data acquisition and preprocessing/processing factors on dyssynchrony parameters. Additionally, this study aimed to standardize dyssynchrony radiomics study according to the Image Biomarker Standardization Initiative (IBSI)[19], which aims to improve reproducibility of the corresponding radiomics studies. This study follows the IBSI reporting guidelines and endeavors to elucidate the correlation between the established vortex formation (with the change of rotations per minute [RPM]), which is denoted by vortex center depth (V-index), and the respective dyssynchrony parameters.

Materials and methods

Simulation phantom

A custom-designed simulation phantom was developed to model the dynamic behavior of blood flow within the left ventricle (LV), mimicking the physiological conditions observed in radionuclide ventriculography (MUGA). The phantom was adapted from a conventional Karmoer® aquarium system (Karmoer® X1 Pro T2, China), with significant modifications including an in-house-designed fluid compartment and alterations to the dosing pump to allow precise control of rotational speed (RPM), flow direction, and turbulence generation (**Figure 1**). These modifications enabled simulation of both laminar and turbulent flow regimes, representing analogs of coordinated and discoordinated ventricular contractions, respectively.

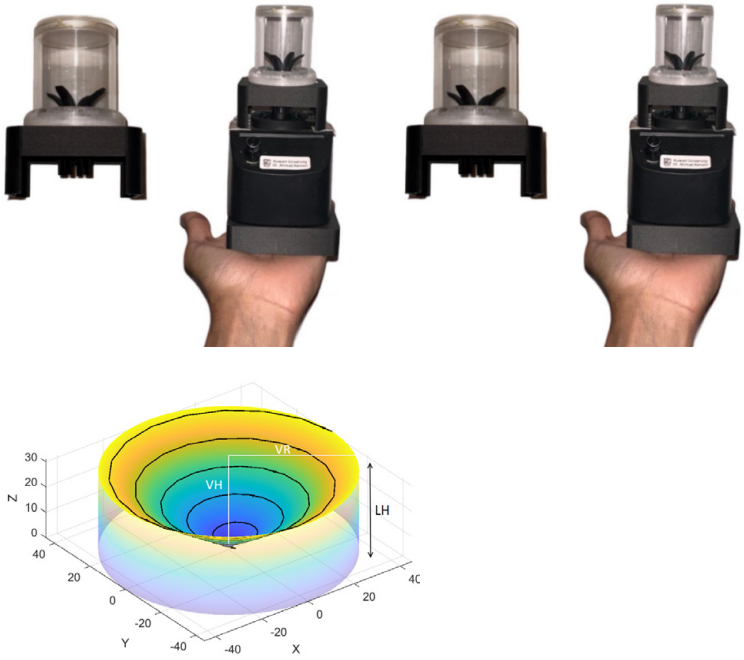


Figure 1. Left: Phantom that was used in this study. Left: at-home designed liquid compartment. Right: overall system with the modified Karmoer dosing system. Right: Simulation generated vortex: The device can be altered to produce various simulations when changing RPM (VH is vortex depth, LH is liquid height (representing marginal level change in liquid when changing RPM) and VR is vortex radius; both are used to calculate V-index (V-index = VR/LH))).

Although the imaging was not ECG-gated, the simulation design emulates gated acquisitions by generating repeatable and phase-consistent dynamic flow patterns, allowing image acquisition of specific simulated "phases" of contraction. In this model, greater temporal discoordination (modeled by variable RPM and flow reversals) is presumed to generate more turbulence, conceptually analogous to increased mechanical dyssynchrony in the LV pool during abnormal ventricular contraction.

To minimize radiation exposure to personnel, the phantom was operated remotely. Experiments were standardized using carefully calibrated Tc-99m activity levels and reproducible imaging protocols. Simulations were run with bidirectional laminar flow (clockwise and counterclockwise) across a range of RPM values (50–750 RPM in 100-RPM increments) to evaluate how directional flow affects derived dyssynchrony parameters. Each simulation used corresponding activity of Tc-99m in a 35 mL solution.

Gating in Nuclear Medicine

Gating in nuclear medicine is a technique used to synchronize image acquisition with the cardiac cycle, typically using an electrocardiogram (ECG) signal. This is especially important in studies like radionuclide ventriculography (MUGA scans) or gated SPECT, where accurate assessment of cardiac motion, function, and timing is required. Gating divides the cardiac cycle into multiple equal time intervals, or frames, allowing for the reconstruction of a time-resolved image series that shows the dynamic motion of the heart. The most common gating modes divide each cardiac cycle into 8 or 16 frames, enabling visualization of systolic and diastolic phases. This improves the temporal resolution of functional parameters like ejection fraction, wall motion, and ventricular synchrony.

Frame Time Calculation

To calculate the frame time (duration of each frame), it is necessary to know the average length of a cardiac cycle, typically represented by the R-R interval (the time between two consecutive R-waves on the ECG). For example, if the patient has a heart rate (HR) of 75 beats per minute (bpm), the $R-R$ interval is:

$$R-R \text{ interval} = \frac{60 \text{ seconds}}{\text{HR}} = \frac{60}{75} = 0.8 \text{ seconds} \left(800 \text{ ms}\right)$$

Then, for 8-frame gating:

$$\text{Frame time} = \frac{800 \text{ ms}}{8} = 100 \text{ ms per frame}$$

And for 16-frame gating:

$$\text{Frame time} = \frac{800 \text{ ms}}{16} = 50 \text{ ms per frame}$$

So, with higher frame numbers (e.g., 16), each frame represents a shorter portion of the cardiac cycle, offering better temporal resolution, but requiring higher count statistics to maintain image quality.

Vortex parameters

Before initiating imaging and with the same liquid and same volume (V=35 mL), vortex dimensions were measured using a custom-made device following the caliper principle. V-indices were measured for every RPM setting.

Data acquisition and simulations

Dynamic images were acquired using a GE Discovery NM 630 gamma camera. The aim was to evaluate how flow pattern irregularities – analogous to mechanical dyssynchrony – affect image-derived synchrony parameters, including entropy, synchrony index, approximate entropy (ApEn), and bounded ApEn. To mimic the temporal characteristics of gated nuclear medicine imaging, particularly radionuclide ventriculography, 64 dynamic acquisitions were performed using a full factorial experimental design. All images were 128*128. This design combined four rotational velocities (0, 50, 150, 250, and 350 RPM), four frame rates (100, 200, 400, and 600 frames per minute), four activity concentrations (37, 29.5, 18.5, and 7.4 MBq (All activity groups were prepared in a fixed volume of 35 mL), respectively), and bidirectional flow (clockwise and counterclockwise). Although our imaging setup was not ECG-gated, the dynamic flow patterns were controlled and repeatable, allowing the simulated data to represent analogs of gated images at different points in the cardiac cycle (see **Table 1 and Ap-**

Table 1. Representative settings for turbulent flow simulations

Series	N[1] Phases	Phase direction PD[2] (PD1, PD2 …)	Phase RPM PRPM[3] (PRPM1, PRPM2 ….)	Phase time PT[4] (PT1, PT2 …)
Turb1	2	1, 0	450, 450	1, 1
Turb2	3	1, 1, 0	450, 700, 650	1, 1, 1
Turb3	4	1, 1, 0, 0	450, 700, 650,750	1, 0.5, 0.1, 6
Turb4	5	1, 0, 1, 1	750, 700, 700, 650	2, 4, 1, 0.3, 3
Turb5	6	1, 0, 1, 1, 0, 1	700, 750, 450, 750, 650	4, 1, 0.5, 8, 0.8,1
Turb6	7	1, 1, 0, 0, 1, 0, 0	750, 700, 750, 450, 650, 000, 000	4, 1, 5, 0.8, 0.8, 1, 0.4
Turb7	14	1, 1, 0, 0, 1, 0, 0, 1, 0, 1, 1, 0, 1, 0	750, 700, 750, 450, 650, 650, 750, 700, 750, 450, 750, 700, 450, 650	4, 1, 5, 8, 0.8, 1, 0.4, 4, 1, 0.5, 8, 0.8, 1, 2

N[1] represents phase, PD[2] represents the corresponding direction of the rotation, PRPM[3] represents the corresponding phase revolution per minute, and PT[4] represents the corresponding phase time.

pendix 1). The selected frame rates correspond to temporal resolutions of 600 ms (100 frames/min) to 100 ms (600 frames/min), similar to the range of frame durations used in 8-frame (e.g., 100 ms per frame) and 16-frame (e.g., 50 ms per frame) gating protocols for heart rates around 75 bpm. This approach enabled us to analyze how varying flow velocities and temporal resolutions influence dyssynchrony-like parameters – such as entropy, synchrony index, approximate entropy (ApEn), and bounded ApEn – under simulated conditions resembling ventricular contraction synchrony and asynchrony. The factorial design ensured a robust dataset for evaluating the impact of each variable on imaging outcomes, reproducibility, and parameter sensitivity.

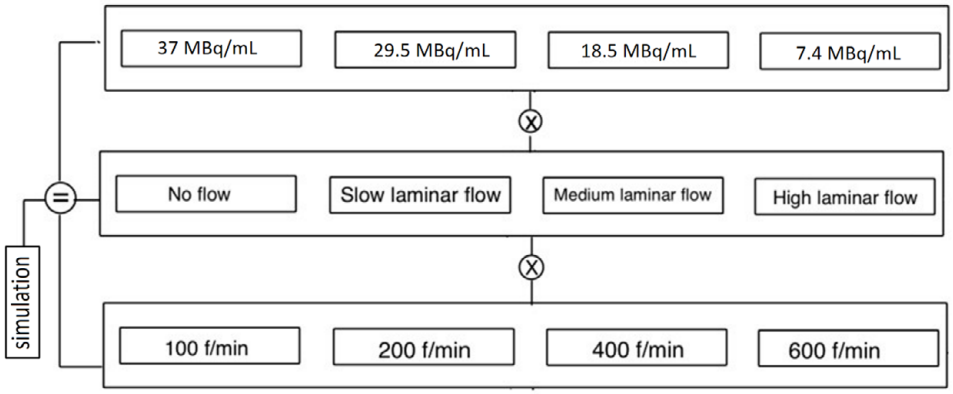


Figure 2. Combinations of simulations used during the experiment, including the range of simulated cardiac flows from no flow (0 RPM) to fast laminar flow (750 RPM). The images vary in radioactive concentrations of ^{99m}Tc Pertechnetate (7.4–37 MBq) and frame rates (100–600 frames/min), offering a comprehensive view of cardiac system dynamics under diverse conditions.

While conventional gated nuclear medicine imaging typically uses 8-16 frames per cardiac cycle, we employed higher frame rates (up to 600 frames/minute or 10 fps) to enable fine temporal sampling of the simulated flow dynamics. This approach ensures that subtle flow changes (analogous to dyssynchrony) could be captured and analyzed more precisely in a controlled setting (simulations are presented in **Figure 2**).

Image processing

A 2D median filter with a 3×3 kernel was applied to each frame of the dynamic image volume to reduce noise while preserving edge information prior to entropy and synchrony analysis. Derivatization of phase and amplitude images: The MATLAB code generated the phase/amplitude image (I) using the following equation:

$$I(i,j)=tan^{-1}\frac{I_{sin}(i,j)}{I_{cos}(i,j)} \quad (1)$$

where $I_{sin}(i,j)$ and $I_{cos}(i,j)$ are the imaginary and real parts of the complex element, respectively, and can be calculated as:

$$I_{sin}(i,j)=\sum_{k=1}^{T} sin\left[\frac{2\pi}{T}(k-1)\right]\times n(i,j,k) \quad (2)$$

$$I_{cos}(i,j)=\sum_{k=1}^{T} cos\left[\frac{2\pi}{T}(k-1)\right]\times n(i,j,k) \quad (2)$$

where T represents the frames/cycle and $n(i,j,k)$ is the pixel (i.e., (i,j)) of kth frame ($k=1,\ldots,T$) of image I. Then, amplitude image can be calculated as:

$$I(i,j)=\sqrt{I_{cos}(i,j)^2+I_{sin}(i,j)^2} \quad (3)$$

The phase images were used to derive entropy parameters.

Synchrony calculation

This algorithm determines synchrony by utilizing a phantom-phase image histogram. It employs a fast Fourier transformation function for each pixel throughout the frames, corresponding to the time-activity curve of each pixel. Every pixel in the image is allocated an angle based on its time delay relative to the frame number. Subsequently, a phase histogram is generated. The magnitude of each vector (representing each pixel) was calculated using the formula denoted as **Equation 5**. Synchrony values can be calculated as follows:

$$S=\frac{\left|\sum_{i=1}^{N} v_i\right|}{\sum_{i=1}^{N}\left|V_i\right|} \quad (4)$$

where v_i is the vector and V_i is the scalar number of pixels in the ROI.

Entropy

Entropy serves as a measure of uncertainty or disorder and reflects the temporal discoordination of ROI such as flow changes. It is expressed as follows:

$$E=\frac{-\sum_{i=1}^{M} P_i \log_2(P_i)}{-\log_2 M} \quad (5)$$

where M stands for the number of phase angles (histogram bins) in the ROI, and Pi is the specific phase angle occurrence frequency (frequency of histogram bin i). Practically, Lower entropy values indicate laminar predictable flow (i.e., temporal coordination) and higher entropy values indicate more tendency toward turbulency and temporal discoordination.

ApEn

ApEn is used to determine the level of consistency, correlation, or endurance within the flow system. It calculates the probability that a sequence of data points of certain length (m) will remain similar within a defined tolerance (r) at a subsequent point in a series. ApEn can be calculated as follows:

$$ApEn=-(N-m)^{-1}\sum_{i=1}^{N-m} ln\left[\frac{c_{i^{m+1}}(r)}{c_{i^m}}\right] \quad (6)$$

where m is sequence length (i.e., the group of pixel values), N is the length of data (i.e., the length of pixel values), and tolerance $c_{i^{m+1}}(r)$ is the conditional probability. The tolerance determines the sequence involved in the next element (i.e., when a sequence falls within the tolerance level, the next data point will be involved and counted at that level). A tolerance comparison was conducted for every m and repeated with $m+1$ to estimate c_{i^m} and $c_{i^{m+1}}$. It should be noted that m value =2 and r value =1 in all simulation experiments.

Bounded-ApEn

Bounded-ApEn uses the tolerance value r . This can be calculated by considering the standard deviation of $e(i)$. The ε is not incorporated in the calculation of bounded-ApEn but used for quality control of the parameter. Bounded-ApEn is calculated as follows:

$$Bounded\,(ApEn) = ApEn(e, m, r) \quad (7)$$

Equation 7 is similar to that used for ApEn derivation but considers the e value. Further details of the mathematical algorithm bounded process and the theoretical aspects of bounded-ApEn have been previously reported[20,21]. It should be noted that e represents a normalized difference signal derived from the input signal (for more details check data availability section).

Prediction of rotation direction

The predictive power of dyssynchrony parameters was examined using 37 MBq in 35 mL. In this simulation, 25 laminar flow simulations (50, 150, 250, 350, 450, 550, 650, and 750 RPM in clockwise and anti-clockwise rotations) were run using the Karmoer device. Six other turbulent flow simulations were also conducted according to the setting described in **Table 1**.

Statistical analysis

Data from different simulations (different RPM, count rate, frame rate, and rotation direction) were compared for differences in means (using suitable parametric or non-parametric tests) and were analyzed for correlation and agreement using Pearson's/Spearman's correlation, multiple linear regression and logistic regression. Tukey's honest significant difference was used to examine the relationship between dyssynchrony and other dependent variables. Furthermore, the impact of independent variables (different RPM, count rate, frame rate, and reading direction) on dyssynchrony readings was investigated. The stepwise selection of terms was performed with α=0.15 for entry and removal. Receiver operating characteristic (ROC) curves were generated to analyze and compare the outcomes of different simulation models.

Results

All results, including those that did not reach statistical significance, are provided in the supplementary material for transparency and completeness. Images were subcategorized into four count rate groups: Group 1: 37 MBq, Group 2: 29.5 MBq, Group 3: 18.5 MBq for the analyses and Group 4: 7.4 MBq .Group 4 was excluded from analysis due to the relatively lower count rate and noise. Examples of the acquired images are illustrated in **Figure 3**.



Figure 3. Represent frames of dynamic images from anterior view (left image) and lateral (right image). All activity groups were prepared in a fixed volume of 35 mL.

Vortex parameters

The V-index is the ratio of the vortex center depth to the marginal level of the liquid. V-indices were measured for each RPM, and the results are presented in **Table 2**. See **Appendix 2** for simulation representations and corresponding V-index.

Table 2. RPM of the device with the corresponding vortex depth (V-index).

RPM	50	150	250	350	450	550	650	750
V-index	0.06	0.13	0.18	0.24	0.29	0.38	0.50	0.57

Group 1: 37 MBq

A substantial negative correlation was observed between entropy values and frame rates (r=-0.991, p=0.001). However, a strong positive correlation was found between the frame rate and synchrony measures (r=0.520, p=0.009).

Group 2: 29.5 MBq

A normal distribution of entropy values was observed for all readings. ANOVA results indicated comparable entropy values across all entropy readings in this group (F [5, 138]<0.001, p=1). Furthermore, no correlation was detected between entropy values, frame rates, device speed (flow rate), or total gray count within the ROI.

Group 3: 18.5 MBq

Several significant positive linear relationships were observed, particularly between the frame rate and ApEn (r=0.625, p=0.001), frame rate and gray count (r=0.801, p<0.001), and frame rate and pixel count (r=0.975, p<0.001). A significant correlation was observed between the pixel count and bounded-ApEn (r=-0.446, p=0.029).

Prediction of rotation direction using ROC curve

A significant difference was observed in the bounded-ApEn values between the clockwise and counterclockwise simulations (p = 0.000085 (95%CI is 0.13 - 0.24)) (**Figure 4**). **Figure 5** presents the ROC curve for the classifier's performance in distinguishing between clockwise and anti-clockwise simulations. The curve demonstrates a high level of accuracy, as evidenced by the AUC of 0.96. This value indicates excellent discrimination ability between clockwise and anti-clockwise directions, with the classifier achieving high sensitivity while maintaining a low false positive rate. Bounded-ApEn was able to significantly discriminate directions of the flow (p = 0.03).

Flow pattern prediction using logistic regression

This simulation and corresponding analysis were only performed in Group 1 (37 MB) only to avoid noise interference.

Turbulent vs. laminar flow

The logistic regression analysis was used to examine the relationship between turbidity and bounded-ApEn using a logit link function on a dataset of 24 observations. The response variable, turbidity, was categorized as either an event (1) (laminar) or non-event (0) (turbulence), with 8 events and 16 non-events. The regression model, Y' = 21.4 - 51.4 × bounded-ApEn, yielded a coefficient of -51.4 for bounded-ApEn (SE =29.4, Z=-1.75, p=0.080), indicating a negative association, although not significant at the 0.05 level. The odds ratio for bounded-ApEn was 0.00001 (95% CI: 0.000001, 450.7405). Logistic regression analysis was used to examine the relationship between flow pattern (laminar vs turbulence) and bounded-ApEn. The model demonstrated a deviance R^2 of 51.71%, adjusted R^2 of 45.17%, and an AUC of 0.94 (**Figure 6**) signifying excellent predictive performance. Goodness-of-fit tests, including the deviance (x2= 14, p=0.88), Pearson's (x2=12, p=0.94), and Hosmer–Lemeshow (x2=3, p=0.96) tests, indicated that the model fits the data well.

Regression between V-index and ApEn

The regression analysis was performed to examine the relationship between V-index and two predictors: ApEn and bounded-ApEn. A 10-fold cross-validation method was employed, along with stepwise selection of terms (α to enter, 0.15; α to remove, 0.15). The resulting regression equation was V-index = -0.0548 - 1.785 × ApEn + 1.829 × bounded-ApEn. The coefficients for ApEn and bounded-ApEn were -1.785 (SE=0.505, T-Value=-3.54, p=0.004, VIF=3.76) and 1.829 (SE=0.191, T-Value=9.56, p<0.001, VIF=3.76), respectively, indicating that both variables significantly contribute to the model. The model achieved an R^2 of 93.01%, adjusted R^2 of 91.94%, and predicted R^2 of 88.91%, with a cross-validated R^2 of 89.32%. Analysis of variance confirmed the model's significance (F-Value=86.54, p<0.001), with significant contributions from ApEn (p=0.004) and bounded-ApEn (p<0.001). The model's residual standard error was 0.0245.

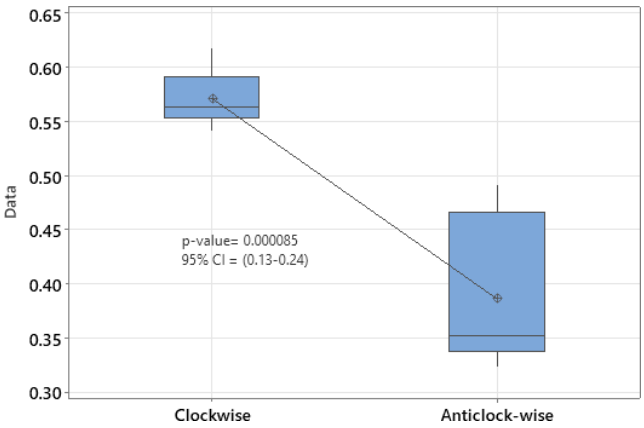


Figure 4. Illustrates the distribution of Bounded-ApEn values (i.e. Data) for clockwise and anti-clockwise flow patterns in the Group 1. The analysis revealed a significant difference between the two flow directions, with a p-value of 0.000085 and a 95% confidence interval of 0.13 to 0.24.

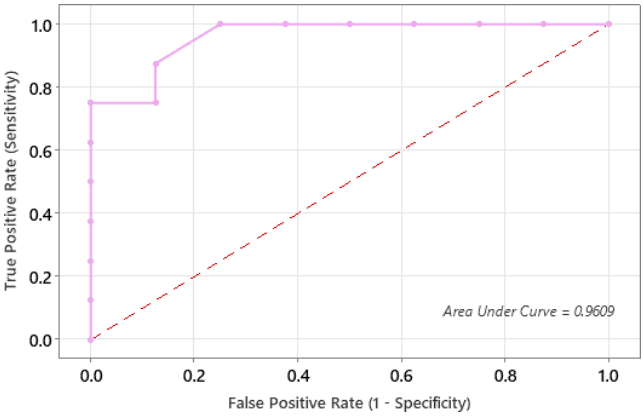


Figure 5. Receiver operating characteristic (ROC) curve of direction discrimination. The curve's proximity to the top-left corner further signifies that the classifier performs well in identifying true positive cases with minimal false positives.

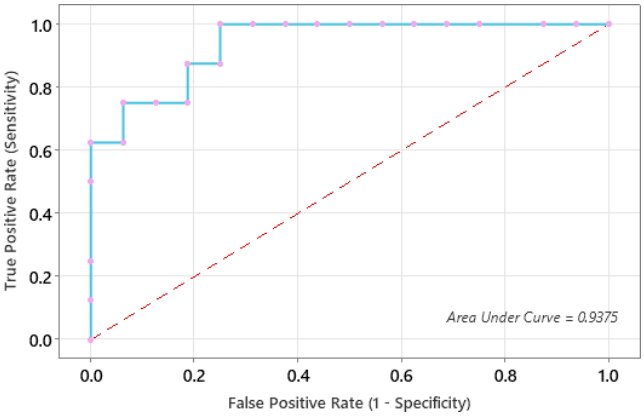


Figure 6. Turbulent vs. laminar flow discrimination curve (ROC) representing discrimination using bounded-ApEn (AUC = 94).

Pairwise comparison (laminar clockwise and laminar anti-clockwise)

The pairwise Pearson's correlations for V-index and RPM were analyzed, revealing significant relationships among the variables. Notably, V-index and RPM showed a strong posi-

tive correlation (r=0.95, p=0.00001), whereas synchrony and RPM demonstrated a strong negative correlation (r=-0.81, p=0.014). Additionally, entropy and V-index were positively correlated (r=0.82, p=0.012), and synchrony and entropy had strong negative correlations (r=-0.89, p=0.003). Strong positive correlations were also observed between ApEn and V-index (r=0.94, p=0.001), as well as bounded-ApEn and V-index (r=0.93, p=0.001). The strong relationships and significant p-values highlight key associations among the variables.

Discussion

Dyssynchrony as radiomics lacks reproducibility and validation, impeding the transition from experimental insights to clinical utility. This challenge is compounded by the absence of consensus-based guidelines and precise definitions for systematically converting complex imaging data to reliable and high-throughput image biomarkers. Addressing these gaps is crucial for ensuring the robustness and credibility of radiomics studies. Consequently, this study aimed to establish a methodological framework for dyssynchrony radiomics, emphasizing the reproducibility, validation, predictability, and establishment of corresponding standardized protocols, to fulfil the full potential of the field in clinical applications without reliability concerns. Although many studies have used entropy and synchrony as clinical markers[1,2,4,6], only a few have discussed the aspects of technical reproducibility, reliability, and standardization. To the best of my knowledge, Jones et al. have published the only previous study on the technical aspects of dyssynchrony. some of the results of the current study are similar to those by Jones et al. in that dyssynchrony parameters demonstrated consistent entropy values across different reading directions, with some inconsistencies in ApEn at lower count rates in our experiment. The sensitivity of ApEn to the tolerance parameter r can influence the resulting values, particularly when r is low, as it increases the impact of self-matches and lowers entropy estimates[9]. This effect may be more pronounced in pixel-based image sequences with shorter data lengths. As noted by Jones et al., this variability necessitates selecting an r value that ensures consistency across the clinical range, leading to the choice of r = 7 in their study. However, this r value seems suitable for radionuclide ventriculography images only[9]. The present study explored a broader range of technical considerations and dyssynchrony parameters compared to those investigated by Jones et al. Specifically, the present study thoroughly examined rotation direction, count rate, and acquisition parameters, providing a more comprehensive analysis of these factors.

This study explored bounded-ApEn for the first time in phantoms and found that it was more consistent than ApEn in terms of direction prediction. The limited effect of pixel matches may be due to the use of log(e), a parameter in the bounded-ApEn, to determine the uncertainty in stochastic models. The time series of some stochastic systems exhibited notable ApEn values, suggesting some predictability. Therefore, assessing the regularity or predictability of signals based solely on ApEn is not feasible. This conclusion is supported by that of previous studies[16,17], which have noted the limitations of directly using ApEn to analyze irregularities in gradually varying patterns with wide-ranging amplitudes, such as those found in electrocardiograph signals. Thus, Wang et al. proposed a log(e) parameter to consider short- and long-term variability in subject systems[20]. In fact, bounded-ApEn has proven its efficacy in predicting stochastic systems and rotation direction in our phantom study.

Jones et al.[5,9,22] comprehensively investigated dyssynchrony; however, they did not fully address how it correlates with deterministic images in terms of count rate, pixel count, and frame rate. Therefore, the present study examined the correlation between these factors and dyssynchrony. Our study found a more complicated relationship between count rate, frame rate and pixel count and dyssynchrony parameters.

Thus, the high degree of correlation observed between different parameters indicates a level of interdependence between these factors. Notably, the frame rate significantly correlated with many factors (e.g. ApEn and bounded-ApEn) across both count rate groups, indicating a potentially influential role. Furthermore, several significant correlations were observed, particularly between the frame rate and different variables (including gray counts), suggesting a degree of complexity in the interactions among these factors, which warrants further investigation of their corresponding effects on dyssynchrony parameters. Understanding the relationships between dyssynchrony parameters and count rate/frame rate may aid the development of more precise and nuanced imaging techniques for dyssynchrony evaluation.

This study aimed to evaluate consistency and reliability of dyssynchrony parameters in the dynamic compartments to fill technical gaps from previous studies[5,8,10,14,22-29]. Additionally, the software developed as part of this study was semiautomated, ensuring reliable data extraction while minimizing the effects of human error and subjective interpretation that may result from inter-rater variability[21]. The statistical methods used in this study helped control the potential sources of variance, thereby ensuring the reproducibility of findings. Moreover, This study distinguished itself through its comprehensive investigation of entropy, synchrony, ApEn, and bounded-ApEn, along with their correlations with parameters such as RPM, count rate, and frame rate. Thus, the robust study design lends credibility and reliability to these findings, setting the groundwork for future exploration of dyssynchrony evaluation.

The logistic regression analysis investigating the relationship between turbulence and Bounded-ApEn revealed a negative association. Clinically, understanding this relationship could be crucial for early detection and management of conditions influenced by turbulent blood-flow (e.g. cardiac valve regurgitation, cardiac infarction and LV thrombus). This insight may enhance our ability to interpret fluid dynamics within the heart compartment, potentially leading to improved patient outcomes by identifying at-risk individuals earlier and tailoring interventions more effectively. Further research is war-

ranted to explore this association in greater depth and validate these findings in larger, more diverse populations.

Detecting turbulence and laminar flow, as well as flow direction in the blood and within heart chambers, offers critical clinical benefits[30-32] by enabling the early detection of cardiovascular diseases, such as atherosclerosis and valve stenosis[33], and guiding surgical and interventional procedures with greater accuracy[34]. Understanding the modeling and flow dynamics helps prevent complications like thrombosis[35] by enabling risk stratification and targeted preventive measures[36]. Additionally, this understanding enhances the design and function of medical devices[36], improves disease monitoring and treatment efficacy, and refines diagnostic imaging techniques. Advanced imaging modalities, such as Doppler ultrasound, phase-contrast MRI, and computational fluid dynamics, can facilitate detailed visualization of blood -flow patterns, aiding in the precise diagnosis of vascular abnormalities and cardiac conditions[34,36]. These capabilities may lead to better patient outcomes through precise diagnostics and personalized treatment plans. The dyssynchrony parameters can be validated and used in such modalities to enhance the predictive power of radiomics.

The logistic regression analysis of the direction and its association with ApEn and bounded-ApEn demonstrated significant effects for both predictors. The model yielded an AUC of 0.96, indicating excellent predictive performance in case of bounded-ApEn. With significant, the analysis suggests that these predictors are robust indicators of direction. Clinically, these findings can be instrumental in predicting directional changes in physiological parameters, thereby assisting in the diagnosis and treatment of conditions where the directionality of physiological signals is crucial, such as in blood-flow patterns and cardiac-function assessments.

The regression analysis examining the relationship between V-index and predictors ApEn/bounded-ApEn showed both variables to be significant contributors to the model. The high R^2 (93.01%) and significant p-values for both predictors underscore their importance. Clinically, these findings suggest that ApEn and bounded-ApEn are valuable indicators for depth-related physiological measurements, potentially enhancing the accuracy of diagnostic procedures and therapeutic strategies that depend on precise depth measurements, such angiography operations especially in pediatric patients suffering from congenital problems[36–38].

The pairwise Pearson's correlation analysis revealed significant relationships among several variables, including strong positive correlations between ApEn and V-index (p=0.935). These findings highlight key associations with potential clinical relevance. For instance, associations involving ApEn may provide insights into the complexity and predictability of physiological signals, potentially informing more nuanced patient -management strategies. In fact, the formation of diastolic vortices in the LV is believed to play a crucial role in optimizing blood pumping efficiency. Conversely, Disruptions in vortex formation have been linked to various left ventricular pathologies[39-40] and dyssynchrony parameters might permit non-invasive prediction of such conditions

Limitations

First, a fixed-shape phantom was used, which restricted the ability to explore the effects of different geometries on flow characteristics of the radioactive liquid system. This limitation may restrict the generalizability of these findings to systems of varying shapes and sizes. Second, the experiments were constrained to a maximum activity of 37 MBq, which may affect the applicability of these results to scenarios involving higher radioactivity and corresponding count rates. Third, the changes in dynamic and gated protocols were not considered, which were outside the study scope. Therefore, these findings may not represent the behavior of the system under different operational conditions, which is crucial for a comprehensive understanding of the dynamics of radioactive liquid systems in various clinical and research settings. This study does not replicate myocardial wall motion or use ECG gating. Instead, the phantom provides a programmable analog for assessing temporal irregularities in flow, mimicking features of dyssynchrony. While not representing a specific clinical test, this setup supports signal processing investigations under controlled dynamic conditions. Further validation in actual gated imaging scenarios is needed before clinical application.

Conclusion

Bounded approximate entropy have discriminative power toward rotation direction (clockwise vs anti-clock-wise) and flow pattern (laminar vs turbulent). The presented correlations among entropy-related parameters and factors such as RPM, count rate, rotation direction and frame rate constitute foundational findings for further research into cardiac imaging and dyssynchrony evaluations. The analyses indicate significant associations between potential key physiological parameters (e.g. Vorticity) and clinical outcomes, highlighting the potential for these predictors (e.g. bounded-ApEn) to enhance diagnostic accuracy and therapeutic strategies in managing conditions influenced by blood -flow patterns and physiological signal directionality. These findings underscore the importance of incorporating these predictors into clinical practice for improved patient care and management strategies.

Funding

This work was supported and funded by Kuwait University, Kuwait (Grant No. ZN07/22).

Disclosures

There are no financial conflicts of interest to disclose.

Acknowledgments

This work was supported by a research grant (ZN07/22) from Kuwait University. The author wish to express his gratitude to Mariam Alenezi, Asiddiq Kalid, and Mahdi Alajmi for their technical expertise and effort in the image acquisition process. The facilitation of this research was made possible by the dedicated efforts of the clinical team, under the guidance of Mohammed Alshaheen, and the technical team, with coordination from Qamar Almutawa'. Their contributions were vital to the completion of this study. Mishari Aljandal provided a limited support in phantom setup.

Key points

QUESTION: Do dyssynchrony parameters in laminar and turbulent flow compartments differ under different image acquisition and processing settings?

PERTINENT FINDINGS: Bounded approximate entropy have discriminative power toward rotation direction (clockwise vs anti-clockwise) and flow pattern (laminar vs turbulent). IMPLICATIONS: These findings may support future development of cardiac dyssynchrony assessments in research and clinical settings and might help in hemodynamic evaluation.

Data availability statement

All data, images and codes are available at: https://github.com/ahmaxiom/dyssynchrony

References

1. Nagueh SF. Mechanical dyssynchrony in congestive heart failure: diagnostic and therapeutic implications. J Am Coll Cardiol. 2008;51:18-22. Doi: 10.1016/j.jacc.2007.08.052
2. Polidori T, De Santis D, Rucci C, et al. Radiomics applications in cardiac imaging: a comprehensive review. Radiol med. 2023;128(8):922-933. doi:10.1007/s11547-023-01658-x
3. Sabouri M, Hajianfar G, Hosseini Z, et al. Myocardial Perfusion SPECT Imaging Radiomic Features and Machine Learning Algorithms for Cardiac Contractile Pattern Recognition. J Digit Imaging. 2022;36(2):497-509. doi:10.1007/s10278-022-00705-9
4. Cook GJR, Azad G, Owczarczyk K, Siddique M, Goh V. Challenges and Promises of PET Radiomics. International Journal of Radiation Oncology*Biology*Physics. 2018;102(4):1083-1089. doi:10.1016/j.ijrobp.2017.12.268
5. Khandoker AH, Palaniswami M, Begg RK. A comparative study on approximate entropy measure and poincaré plot indexes of minimum foot clearance variability in the elderly during walking. J NeuroEngineering Rehabil. 2008;5(1). doi:10.1186/1743-0003-5-4
7. Li X, Zheng D, Zhou S, Tang D, Wang C, Wu G. Approximate entropy of fetal heart rate variability as a predictor of fetal distress in women at term pregnancy. Acta Obstet Gynecol Scand. 2005;84(9):837-843. doi:10.1111/j.0001-6349.2005.00773.x
8. Pincus SM. Approximate entropy as a measure of system complexity. Proc Natl Acad Sci USA. 1991;88(6):2297-2301. doi:10.1073/pnas.88.6.2297
9. Jones KA, Paterson CA, Hamilton DJ, et al. Optimising approximate entropy for assessing cardiac dyssynchrony with radionuclide ventriculography. Biomedical Signal Processing and Control. 2021;68:102703. doi:10.1016/j.bspc.2021.102703
10. O'Connell JW, Schreck C, Moles M, et al. A unique method by which to quantitate synchrony with equilibrium radionuclide angiography. Journal of Nuclear Cardiology. 2005;12(4):441-450. doi:10.1016/j.nuclcard.2005.05.006
11. Jimenez-Angeles L, Medina-Banuelos V, Valdes-Cristerna R, Vallejo E. Analysis of Ventricular Contraction by Factorial Phase Imaging with Equilibrium Radionuclide Angiography. 2006 International Conference of the IEEE Engineering in Medicine and Biology Society. Published online August 2006:1081-1084. doi:10.1109/iembs.2006.259252
12. Nichols KJ, Van Tosh A, Wang Y, De Bondt P, Palestro CJ, Reichek N. Automated detection of left ventricular dyskinesis by gated blood pool SPECT. Nuclear Medicine Communications. 2010;31(10):881-888. doi:10.1097/mnm.0b013e32833d82ff
13. Lalonde M, Wells RG, Birnie D, Ruddy TD, Wassenaar R. Development and optimization of SPECT gated blood pool cluster analysis for the prediction of CRT outcome. Med Phys. 2014;41(7):072506. doi:10.1118/1.4883881
14. Johnson CJ, Roberts JD, James JH, et al. Comparison of radionuclide angiographic synchrony analysis to echocardiography and magnetic resonance imaging for the diagnosis of arrhythmogenic right ventricular cardiomyopathy. Heart Rhythm. 2015;12(6):1268-1275. doi:10.1016/j.hrthm.2015.02.033
15. Sullivan DC, Obuchowski NA, Kessler LG, et al. Metrology Standards for Quantitative Imaging Biomarkers. Radiology. 2015;277(3):813-825. doi:10.1148/radiol.2015142202
16. Goldberger AL, Peng CK, Lipsitz LA. What is physiologic complexity and how does it change with aging and disease? Neurobiology of Aging. 2002;23(1):23-26. doi:10.1016/s0197-4580(01)00266-4
17. Xu Y, Ma X, Ning X. Estimation of ApEn for short-term HFECG based on multi-resolution analysis. Physica A: Statistical Mechanics and its Applications. 2007;376:401-408. doi:10.1016/j.physa.2006.10.055
18. Kuronuma K, Miller RJH, Van Kriekinge SD, et al. Incremental prognostic value of stress phase entropy over standard PET myocardial perfusion imaging variables. Eur J Nucl Med Mol Imaging. 2023;50(12):3619-3629. doi:10.1007/s00259-023-06323-z
19. Zwanenburg A, Vallières M, Abdalah MA, et al. The Image Biomarker Standardization Initiative: Standardized Quantitative Radiomics for High-Throughput Image-based Phenotyping. Radiology. 2020;295(2):328-338. doi:10.1148/radiol.2020191145
20. Wang Y, Lu S. A bounded random process model and its application in heart rate variability analysis. Intl J Phys Sci. 2011;6:651-659.
21. Alenezi A. MATLAB central. https://www.mathworks.com/matlabcentral/profile/authors/27389582?detail=fileexchange. Accessed August 5, 2023.

22. Jones KA, Small AD, Ray S, et al. Radionuclide ventriculography phase analysis for risk stratification of patients undergoing cardiotoxic cancer therapy. Journal of Nuclear Cardiology. 2022;29(2):581-589. doi:10.1007/s12350-020-02277-z

23. Singh H, Singhal A, Sharma P, Patel CD, Seth S, Malhotra A. Quantitative assessment of cardiac mechanical synchrony using equilibrium radionuclide angiography. Journal of Nuclear Cardiology. 2013;20(3):415-425. doi:10.1007/s12350-013-9705-3

24. Juarez-Orozco LE, Monroy-Gonzalez A, Prakken NHJ, et al. Phase analysis of gated PET in the evaluation of mechanical ventricular synchrony: A narrative overview. Journal of Nuclear Cardiology. 2019;26(6):1904-1913. doi:10.1007/s12350-019-01670-7

25. Vallejo E, Jiménez L, Rodríguez G, Roffe F, Bialostozky D. Evaluation of Ventricular Synchrony with Equilibrium Radionuclide Angiography: Assessment of Variability and Accuracy. Archives of Medical Research. 2010;41(2):83-91. doi:10.1016/j.arcmed.2010.02.003

26. Fauchier L, Marie O, Casset-Senon D, Babuty D, Cosnay P, Fauchier JP. Interventricular and intraventricular dyssynchrony in idiopathic dilated cardiomyopathy. Journal of the American College of Cardiology. 2002;40(11):2022-2030. doi:10.1016/s0735-1097(02)02569-x

27. Dauphin R, Nonin E, Bontemps L, et al. Quantification of Ventricular Resynchronization Reserve by Radionuclide Phase Analysis in Heart Failure Patients. Circ: Cardiovascular Imaging. 2011;4(2):114-121. doi:10.1161/circimaging.110.950956

28. Marcassa C, Campini R, Verna E, Ceriani L, Giannuzzi P. Assessment of cardiac asynchrony by radionuclide phase analysis: Correlation with ventricular function in patients with narrow or prolonged QRS interval. European J of Heart Fail. 2007;9(5):484-490. doi:10.1016/j.ejheart.2007.01.002

29. Fukunaga T, Sanui K, Kadokami T, Sasaki M. Influences of radionuclides on left ventricular phase analysis of gated myocardial perfusion single-photon emission computed tomography images in ischemic heart disease. Ann Nucl Med. 2021;35(6):735-743. doi:10.1007/s12149-021-01615-6

30. Domenichini F, Pedrizzetti G. Asymptotic Model of Fluid–Tissue Interaction for Mitral Valve Dynamics. Cardiovasc Eng Tech. 2014;6(2):95-104. doi:10.1007/s13239-014-0201-y

31. Jahanzamin J, Fatouraee N, Nasiraei-Moghaddam A. Effect of turbulent models on left ventricle diastolic flow patterns simulation. Computer Methods in Biomechanics and Biomedical Engineering. 2019;22(15):1229-1238. doi:10.1080/10255842.2019.1655642

32. Varghese SS, Frankel SH. Numerical Modeling of Pulsatile Turbulent Flow in Stenotic Vessels. Journal of Biomechanical Engineering. 2003;125(4):445-460. doi:10.1115/1.1589774

33. Saqr KM, Tupin S, Rashad S, et al. Physiologic blood flow is turbulent. Sci Rep. 2020;10(1). doi:10.1038/s41598-020-72309-8

34. Fraser KH, Taskin ME, Griffith BP, Wu ZJ. The use of computational fluid dynamics in the development of ventricular assist devices. Medical Engineering & Physics. 2011;33(3):263-280. doi:10.1016/j.medengphy.2010.10.014

35. Tobin N, Manning KB. Toward modeling thrombosis and thromboembolism in laminar and turbulent flow regimes. Numer Methods Biomed Eng. 2022;38(10). doi:10.1002/cnm.3638

36. Qian K xi. Haemodynamic approach to reducing thrombosis and haemolysis in an impeller pump. Journal of Biomedical Engineering. 1990;12(6):533-535. doi:10.1016/0141-5425(90)90066-v

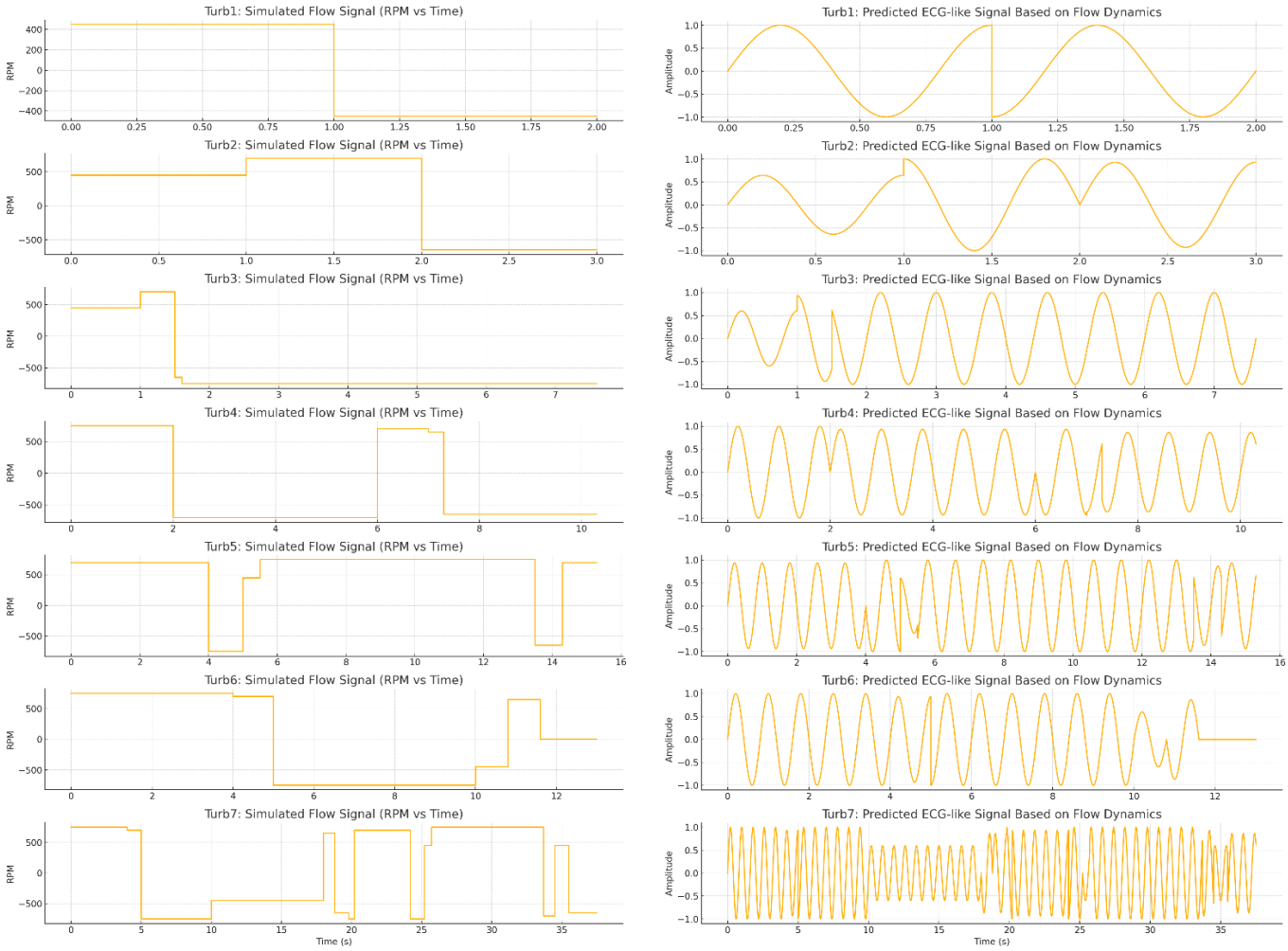
37. Kheradvar A, Rickers C, Morisawa D, Kim M, Hong GR, Pedrizzetti G. Diagnostic and prognostic significance of cardiovascular vortex formation. Journal of Cardiology. 2019;74(5):403-411. doi:10.1016/j.jjcc.2019.05.005

38. Marchese P, Cantinotti M, Van den Eynde J, et al. Left ventricular vortex analysis by high-frame rate blood speckle tracking echocardiography in healthy children and in congenital heart disease. IJC Heart & Vasculature. 2021;37:100897. doi:10.1016/j.ijcha.2021.100897

39. Elbaz MSM, Calkoen EE, Westenberg JJM, Lelieveldt BPF, Roest AAW, van der Geest RJ. Vortex flow during early and late left ventricular filling in normal subjects: quantitative characterization using retrospectively-gated 4D flow cardiovascular magnetic resonance and three-dimensional vortex core analysis. Journal of Cardiovascular Magnetic Resonance. 2014;16(1):78. doi:10.1186/s12968-014-0078-9

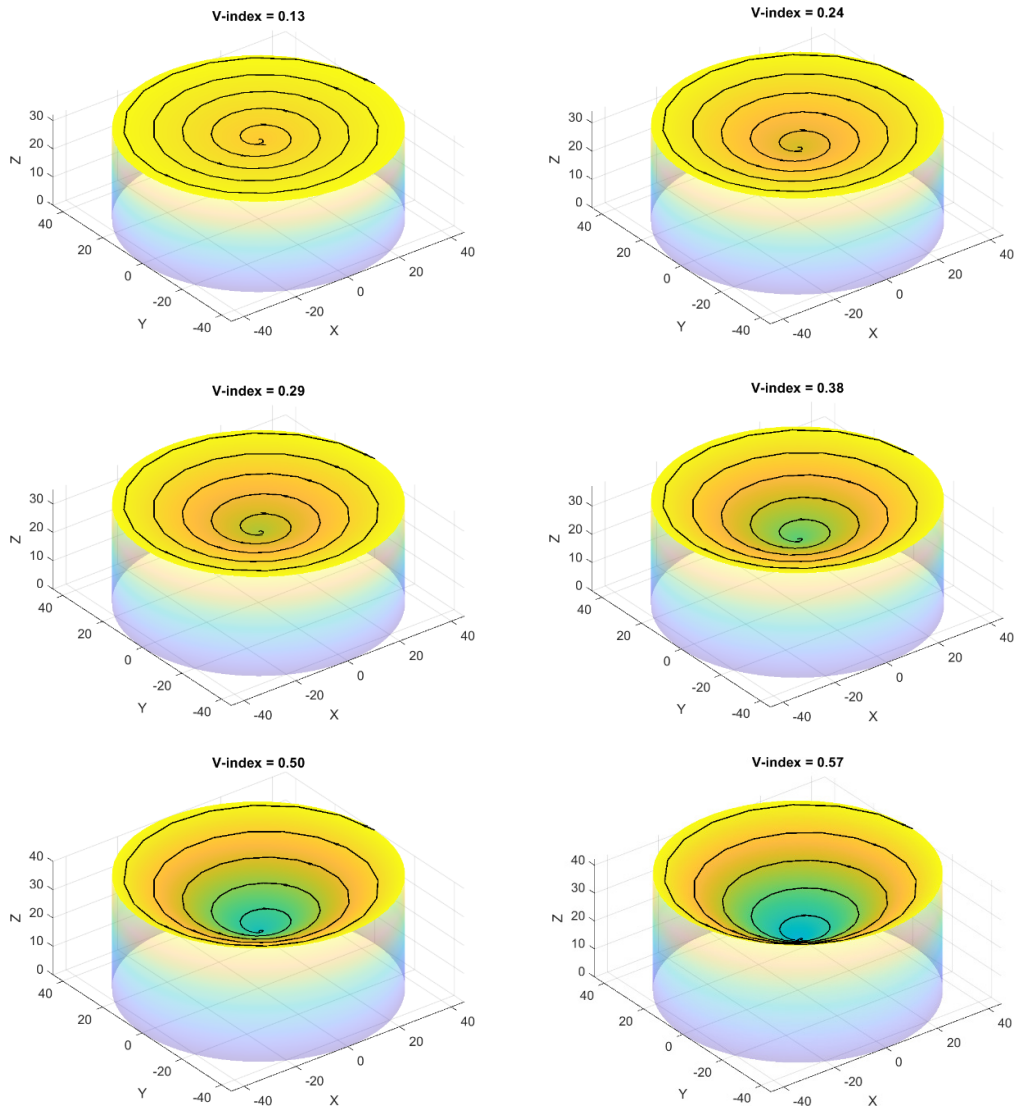
40. Alenezi A, McKiddie F, Nath M, Mayya A, Welch A. 2024. Cardiotoxicity detection tool for breast cancer chemotherapy: a retrospective study. PeerJ Computer Science 12:e2230 https://doi.org/10.7717/peerj-cs.2230

Appendix 1.



Simulated flow dynamics and corresponding predicted ECG-like (not exact ECG) signals for seven turbulent flow scenarios (Turb1–Turb7) using a dynamic phantom model (from Table 1). Left panels show the phase-specific rotational velocity (RPM) profiles over time, with changes in direction and magnitude simulating laminar and turbulent flow patterns. Right panels display the predicted ECG-like signals derived from these flow patterns, mimicking the temporal effects of ventricular contraction synchrony and dyssynchrony. These simulations conceptually replicate gated cardiac imaging by linking mechanical flow variations to electrophysiological signal analogs.

Appendix 2.



Depicts images of various simulations showing changes in RPM and the corresponding V-index. The spiral line is an illustration of the rotation vector. In this simulation images, all directions are anti-clockwise.